JETP Letters, Vol. 80, No. 6, 2004, pp. 426–432. Translated from Pis'ma v Zhurnal Éksperimental'noĭ i Teoreticheskoĭ Fiziki, Vol. 80, No. 6, 2004, pp. 482–488.

Structural and Electronic Transitions in Gadolinium Iron Borate $GdFe_3(BO_3)_4$ at High Pressures

A. G. Gavriliuk[1, 2], S. A. Kharlamova[3], I. S. Lyubutin[2, *], I. A. Troyan[1], S. G. Ovchinnikov[3], A. M. Potseluiko[3], M. I. Eremets[4], and R. Boehler[4]

[1]*Institute of High-Pressure Physics, Russian Academy of Sciences, Troitsk, Moscow region, 142092 Russia*
[2]*Institute of Crystallography, Russian Academy of Sciences, Moscow, 119333 Russia*
[3]*Kirensky Physics Institute, Siberian Division, Russian Academy of Sciences, Krasnoyarsk, 660036 Russia*
[4]*Max-Planck Institut für Chemie, 55020 Mainz, Germany*
**e-mail: lyubutin@ns.crys.ras.ru*
Received July 30, 2004

The optical properties and structure of gadolinium iron borate $GdFe_3(BO_3)_4$ crystals are studied at high pressures produced in diamond-anvil cells. X-ray diffraction data obtained at a pressure of 25.6 GPa reveal a first-order phase transition retaining the trigonal symmetry and increasing the unit cell volume by 8%. The equation of state is obtained and the compressibility of the crystal is estimated before and after the phase transition. The optical spectra reveal two electronic transitions at pressures ~26 GPa and ~43 GPa. Upon the first transition, the optical gap decreases jumpwise from 3.1 to ~2.25 eV. Upon the second transition at $P = 43$ GPa, the optical gap deceases down to ~0.7 eV, demonstrating a dielectric–semiconductor transition. By using the theoretical model developed for a $FeBO_3$ crystal and taking into account some structural analogs of these materials, the anomalies of the high-pressure optical spectra are explained. © *2004 MAIK "Nauka/Interperiodica".*

PACS numbers: 61.50.Ks; 71.27.+a; 71.30.+h; 81.40.Tv

1. INTRODUCTION

A $GdFe_3(BO_3)_4$ crystal belongs to the family of rare-earth borates $RM_3(BO_3)_4$ (R is a rare-earth element, M = Al, Ga, Fe, Sc), which are isostructural to a natural mineral huntite $CaMg_3(CO_3)_4$ [1] and have trigonal symmetry with the space group R32 (D_{3h}^7) [2, 3]. Recently, the nonlinear optical and laser properties of these materials were found [4–6], which attracted great attention from researchers.

The structure of rare-earth iron borates $RFe_3(BO_3)_4$ can be represented in the form of layers perpendicular to the *c*-axis (C_3) and consisting of trigonal RO_6 prisms and lower-size FeO_6 octahedra [2, 3]. The FeO_6 octahedra are connected by their faces and form helical one-dimensional weakly coupled chains elongated along the *c*-axis. Boron atoms form isolated triangles with oxygen atoms, producing BO_3^{3-} groups of two types. Triangles of the type $B(1)O_3$ are connected by their vertices only with the FeO_6 polyhedra, while triangles of the type $B(2)O_3$ are connected by two vertices with different chains of the FeO_6 octahedra and by the third vortex with the RO_6 prism.

The physical properties of rare-earth iron borates are poorly studied, which is mainly explained by the difficulty of growing high-quality crystals, especially for optical studies. The recent measurements [7, 8] of the magnetic susceptibility, magnetization, and heat capacity showed that a $GdFe_3(BO_3)_4$ borate crystal is a compensated antiferromagnetic with the Néel temperature $T_N = 38$ K, and the spin-flop transition occurs in the crystal at a temperature about 10 K. It is assumed that magnetic ordering below T_N concerns only iron ions, whereas the Gd^{3+} ions remain paramagnetic at least down to liquid helium temperature [7]. In addition, quite recently the structural phase transition was also discovered in this crystal at $T = 156$ K [9].

In this paper, we studied the optical properties and change in the structure of a $GdFe_3(BO_3)_4$ crystal at high pressures produced in diamond-anvil cells. We found two phase transitions at pressures ~26 and ~43 GPa accompanied by the jumpwise narrowing of the optical gap and the dielectric–semiconductor transition.

2. EXPERIMENTAL

High-quality transparent, dark green $GdFe_3(BO_3)_4$ crystals were grown from solution in a melt [10]. The crystal lattice parameters at normal pressure are $a = 9.5491(6)$ and $c = 7.5741(5)$ Å.

X-ray diffraction studies at pressures up to 40 GPa were performed with a polycrystalline sample obtained by single-crystal crushing. The sample was studied at room temperature in a diamond-anvil cell in a specialized laboratory setup at the Max-Planck Institut für

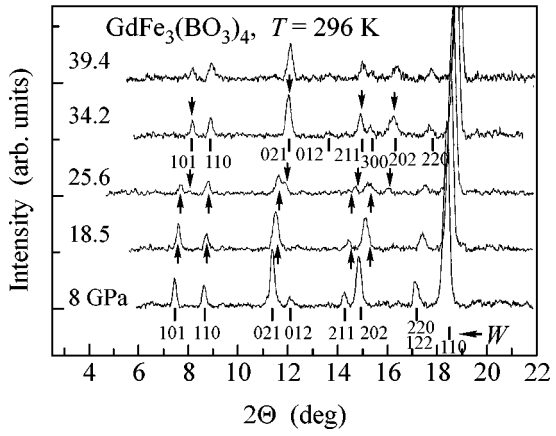

Fig. 1. X-ray diffraction patterns of the $GdFe_3(BO_3)_4$ polycrystal at room temperature at some pressures below and above the phase transition. *W* denotes the position of a reflection from a tungsten gasket.

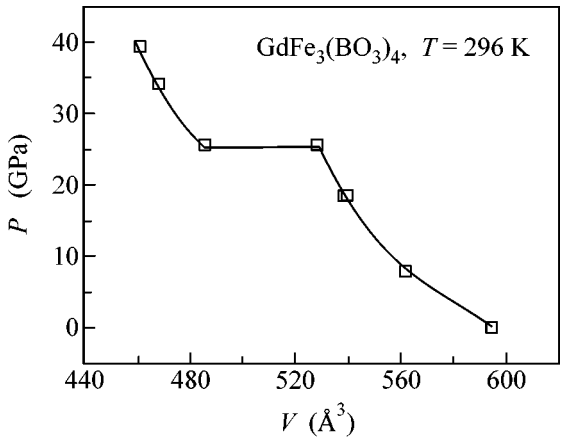

Fig. 2. Baric dependence of the unit cell volume of the $GdFe_3(BO_3)_4$ crystal at room temperature.

Chemie (Mainz, Germany). X-rays were generated by a rotating Mo anode (0.7093 Å) with a special focusing system. Spectra were recorded in the transmission geometry using an Image Plate detector. The high-pressure cell allowed the recording of the spectra in the 30° range of angles 2Θ. The diameter of the diamond anvils was 300 μm, and the diameter of a hole in a tungsten gasket, where a sample was placed, was about 100 μm. Pressure was transmitted to a sample through a PES-5 polyethylsilaxane liquid. To provide quasi-hydrostatic conditions, the working volume of the cell was filled by 1/3 with a sample and by 2/3 with the PES-5 liquid. Pressure was measured by a standard method by the shift of the fluorescence line of ruby.

The optical absorption spectra were measured for a $GdFe_3(BO_3)_4$ crystal at pressures up to 60 GPa at room temperature in the diamond-anvil cell. Diamond anvils of diameter ~400 μm were used. The hole at the center of a rhenium gasket had a diameter of ~120 μm. Measurements were performed for a thin plate of size ~50 × 40 × 15 μm punctured from a massive $GdFe_3(BO_3)_4$ crystal. The light beam was directed perpendicular to the basis plane of the crystal. Pressure was imparted to a sample through a PES-5 liquid providing quasi-hydrostatic compression. A single crystal remained undamaged after the pressure removal. The optical setup for the study of absorption spectra allows one to perform measurements in the visible and near-IR ranges from 0.3 to 5 μm. An FEU-100 photomultiplier was used as a detector in the visible region, while in the near-IR region a germanium diode cooled in liquid nitrogen was used. The light-spot diameter on a sample was ~20 μ. The absorption spectrum was calculated from the expression $I = I_0\exp(-\alpha d)$, where d is the sample thickness, I_0 is the reference signal intensity outside the sample, and α is the absorption coefficient.

3. EXPERIMENTAL RESULTS

3.1. High-pressure X-Ray Studies

The dependence of the X-ray diffraction pattern of a $GdFe_3(BO_3)_4$ crystal on pressure is shown in Fig. 1. As pressure increases, peaks in the diffraction pattern shift in the direction of larger angles, and new peaks appear at $P > 25$ GPa, indicating the transformation of the crystal structure. For $P = 25.6$ GPa, reflections from two coexisting low- and high-pressure phases are observed. This can be caused by incompletely hydrostatic conditions and the presence of a pressure gradient in the cell or by a peculiarity of the first-order phase transition. One can see from Fig. 1 that the main peaks for a new high-pressure phase are identical to those for the low-pressure phase. Therefore, the high-pressure phase was indexed assuming that the crystal symmetry is preserved after the structural phase transition (see Fig. 1). Figure 2 shows the pressure dependence of the unit cell volume for the $GdFe_3(BO_3)_4$ crystal at room temperature calculated using the data presented in Fig. 1. Experimental points for the low-pressure phase were approximated by the Berch–Murnagan equation,

$$P = \frac{3}{2}B_0\left(\frac{V}{V_0}\right)^{-5/3}\left(1-\left(\frac{V}{V_0}\right)^{-2/3}\right) \times\left[\frac{3}{4}(B'-4)\left(1-\left(\frac{V}{V_0}\right)^{-2/3}\right)-1\right]. \quad (1)$$

The approximation gave the bulk modulus $B_0 = 159.5 \pm 6.3$ GPa, its derivative $B' = 4$ (fixed), and unit cell volume at the normal pressure $V_0 = 594.69$ Å^3. After the structural transition at $P = 25.6$ GPa, experi-

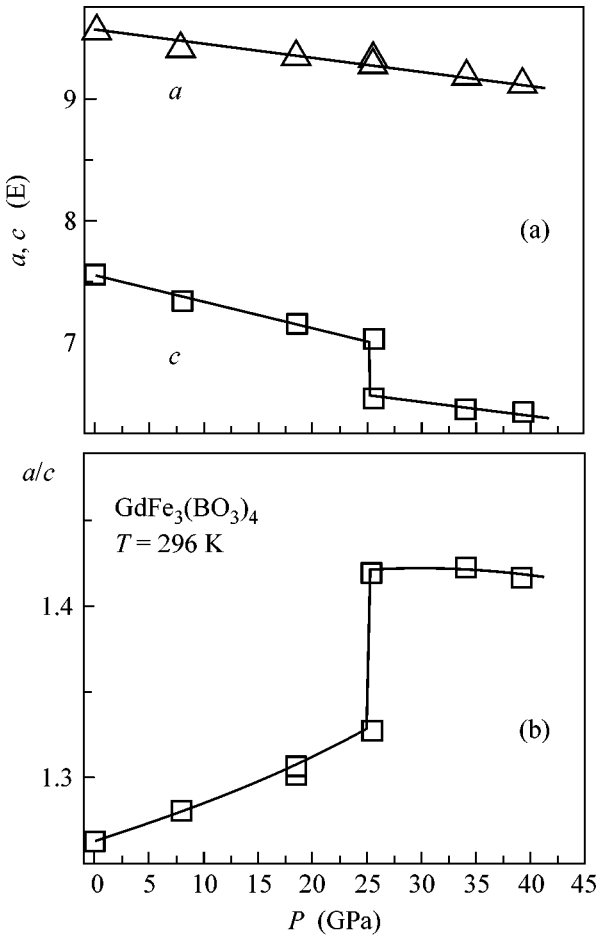

Fig. 3. Baric dependences of the unit cell parameters *a* and *c* in the $GdFe_3(BO_3)_4$ crystal at room temperature (a) and of the *a*/*c* ratio (b).

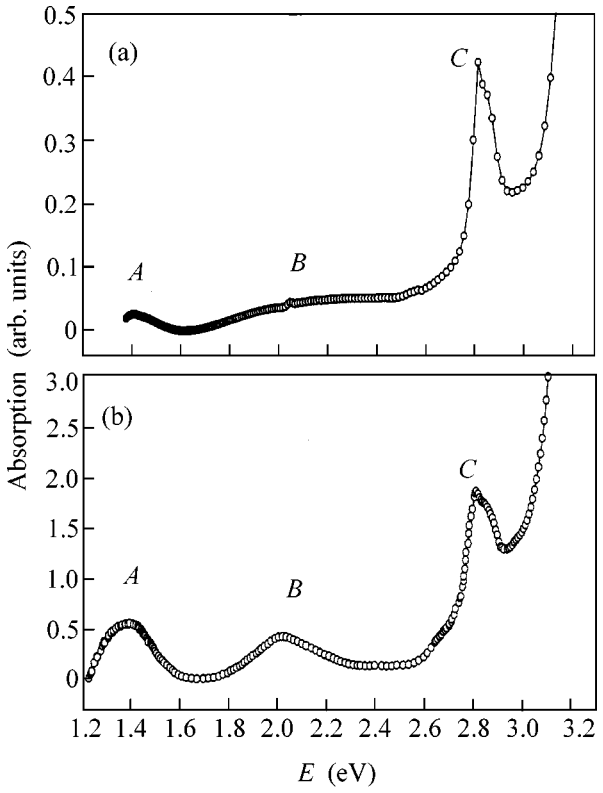

Fig. 4. Absorption spectra of (a) $GdFe_3(BO_3)_4$ and (b) $FeBO_3$ single crystals at normal pressure and room temperature.

mental points for the high-pressure phase were approximated by the modified Birch-Murnagan equation,

$$P + 25.6\ \text{GPa} = \frac{3}{2}B_{26}\left(\frac{V}{V_{26}}\right)^{-5/3}\left(1-\left(\frac{V}{V_{26}}\right)^{-2/3}\right) \times\left[\frac{3}{4}(B'_{26}-4)\left(1-\left(\frac{V}{V_{26}}\right)^{-2/3}\right)-1\right] \quad (2)$$

and we obtained $B_{26} = 219.5 \pm 6.5$ GPa, $B'_{26} = 4$ (fixed), and $V_{26} = 486.022$ Å^3.

Therefore, the structural transition in the $GdFe_3(BO_3)_4$ crystal at $P = 25.6$ GPa is the first-order symmetry-retaining transition accompanied by the ~8% jump in the unit cell volume. Note that the crystal compressibility in the high-pressure phase is higher than that in the low-pressure phase.

Figure 3a shows the pressure dependence of the crystal-lattice parameters. One can see that the structural transition is accompanied by a jumpwise decrease in the parameter *c*, whereas the parameter *a* decreases gradually. Figure 3b shows the pressure dependence of the ratio *a*/*c* of the lattice parameters.

3.2. Optical Absorption Spectra

For measurements at normal pressure, the $GdFe_3(BO_3)_4$ crystals were prepared in the form of thin plates of area ~2 mm^2 and thickness from 42 to 53 μm. The plate plane was oriented parallel or perpendicular to the threefold crystallographic axis C_3, and a light beam was directed perpendicular to the plate. Optical spectra were recorded in the spectral range from 10000 to 40000 cm^{-1} (1.24–4.96 eV) at 300 K. The spectral width of the slit of a grating monochromator was 10 cm^{-1}. The accuracy of measurement of the absorption coefficient was 3%. We found that the absorption spectra were virtually identical for both orientations.

Figure 4 shows the absorption spectrum of the $GdFe_3(BO_3)_4$ crystal at normal pressure at room temperature. For comparison, the absorption spectrum of the well-studied iron borate $FeBO_3$ obtained by us earlier [11] is also presented. We found that the energies of absorption bands of the $GdFe_3(BO_3)_4$ and $FeBO_3$ crystals coincide with an accuracy to tenths of electronvolts. Three groups of absorption bands at 1.4, 2.0, and 2.8 eV were observed. The energy gap determining the

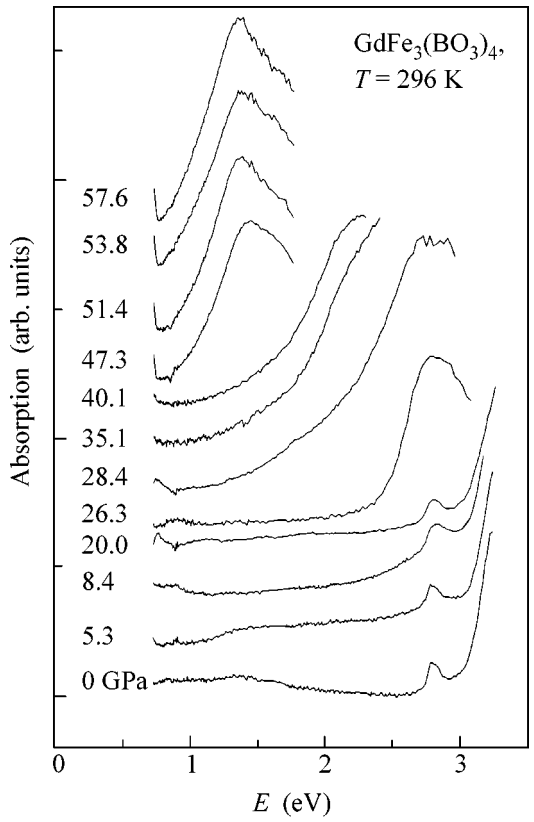

Fig. 5. Absorption spectra of the $GdFe_3(BO_3)_4$ crystal at different pressures at room temperature.

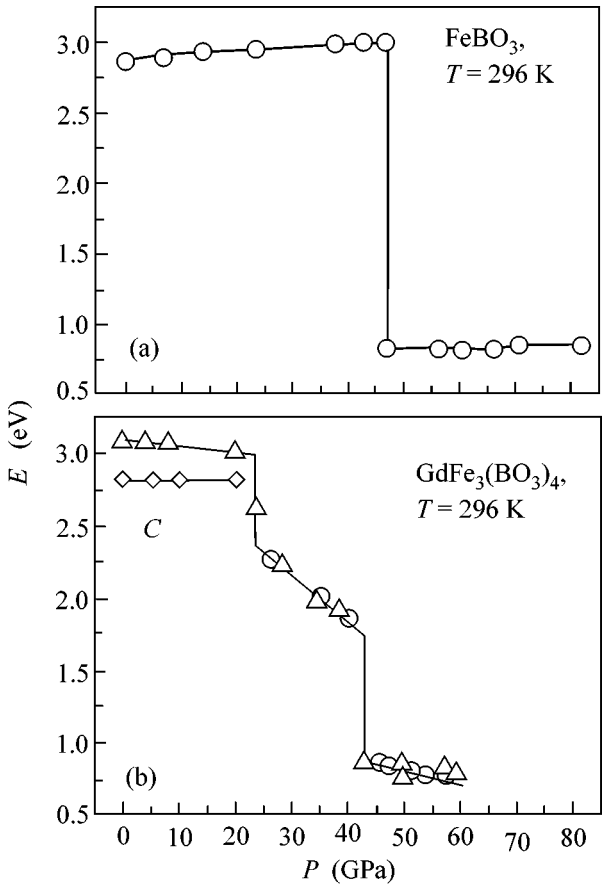

Fig. 6. Baric dependences of the absorption edge in (a) $FeBO_3$ and (b) $GdFe_3(BO_3)_4$ single crystals at room temperature. The triangles and circles for $GdFe_3(BO_3)_4$ correspond to different measurement series; *C* is the absorption band.

fundamental absorption edge in the $GdFe_3(BO_3)_4$ crystal is E_g = 3.1 eV, which is somewhat greater than in $FeBO_3$ (2.9 eV).

The similarity of the absorption bands suggests that the optical properties of $FeBO_3$ and $GdFe_3(BO_3)_4$ coincide in the energy range 1–3 eV, and the three groups of bands *A*, *B*, and *C* (Fig. 4) are caused by the ${}^6A_{1g}({}^6S) \longrightarrow {}^4T_{1g}({}^4G)$, ${}^6A_{1g}({}^6S) \longrightarrow {}^4T_{2g}({}^4G)$, and ${}^6A_{1g}({}^6S) \longrightarrow {}^4A_{1g,\,{}^4E_g}({}^4G)$ *d*–*d* transitions, respectively [11].

To determine the possible contributions from rare-earth ions, we recorded the transmission spectra of the $GdFe_3(BO_3)_4$ crystal of thickness 1.58 mm at 300 K using the InSb and Si detectors [12]. We found that the Gd^{3+} ion has no absorption bands in a broad spectral region up to 32500 cm^{-1} (4 eV). Therefore, the *A*, *B*, and *C* bands in the spectra of $GdFe_3(BO_3)_4$ (Fig. 4) should be assigned to the *d*–*d* transitions in Fe^{3+}, i.e., to the transition from the 5/2 ground state to the 3/2 excited state.

The pressure dependence of the absorption spectrum of the $GdFe_3(BO_3)_4$ crystal is shown in Fig. 5. Before the phase transition at $P \approx 26$ GPa, the position of the *C* band can be distinctly observed. One can see that the energy of this band is virtually independent of pressure in this pressure range, being equal to ~2.8 eV (Fig. 6).

In the critical region near P_{c1} = 26 GPa, the spectrum changes noticeably due to the phase transition described above. In this case, the optical gap decreases jumpwise from ~3 to ~2.25 eV (Fig. 6). In a new phase, the optical gap strongly decreases down to ~1.7 eV with increasing pressure from 26 to 43 GPa (Fig. 6) and then sharply decreases down to ~0.7 eV at the pressure P_{c2} = (43 ± 2) GPa. Therefore, at $P_{c2} \approx 43$ GPa, the second phase transition occurs in the $GdFe_3(BO_3)_4$ crystal with changing electronic structure, and, according to the optical-gap value, this transition can be interpreted as the dielectric–semiconductor transition.

To estimate the pressure P_{met} at which the optical gap vanishes and complete metallization occurs, we approximated the baric dependence of the optical gap after the phase transition at P_{c2} = 43 GPa by the linear function

$$E = E_0\left(1 - \frac{P}{P_{met}}\right). \quad (3)$$

The B–O and Fe–O interionic distances and the optical gap E_g in $GdFe_3(BO_3)_4$ and $FeBO_3$ crystals

	B–O, Å	Fe–O, Å	E_g, eV
$FeBO_3$	1.3790	2.028	2.9
$GdFe_3(BO_3)_4$	1.3676	2.029	3.1

In the absence of additional transitions, the approximation gives $E_0 = (1.31 \pm 0.05)$ eV (E_0 is the effective optical gap in a new phase extrapolated to zero pressure) and $P_{met} = 135 \pm 11$ GPa.

Therefore, we observed two phase transitions accompanied by an optical-gap jump in the $GdFe_3(BO_3)_4$ crystal at $P_{c1} \approx 26$ GPa and $P_{c2} \approx 43$ GPa. The electronic transition at the point $P_{c1} \approx 26$ GPa coincides with the structural transition. It is quite probable that the second electronic transition at $P_{c2} \approx 43$ GPa is also accompanied by the structural transition. However, we could increase pressure only up to 40 GPa in our study and, therefore, could not achieve the second phase transition. Note that after pressure was decreased to the normal value, the single crystal remained undamaged; however, its color changed from dark green to light brown.

Figure 6 also shows the baric dependence of the optical gap in iron borate $FeBO_3$ [13]. The pressure at which the electronic phase transition occurs with a drastic change in the energy gap in $FeBO_3$ is close to the value of P_{c2} for the $GdFe_3(BO_3)_4$ crystal, which again confirms the similarity of the electronic structures of these compounds.

4. DISCUSSION OF RESULTS. COMPARISON OF THE ELECTRONIC STRUCTURE OF IRON BORATES $GdFe_3(BO_3)_4$ AND $FeBO_3$

The absorption spectra show that the electronic structure of the $GdFe_3(BO_3)_4$ crystal is close to that of $FeBO_3$ and is determined in the energy range to 4 eV in the vicinity of the Fermi level by the Fe ion and its environment. The interionic distances Fe–O and B–O in $FeBO_3$ and $GdFe_3(BO_3)_4$ are also close to each other (see table). This allows one to use some theoretical concepts developed for $FeBO_3$ [11, 13, 14] and $GdFe_3(BO_3)_4$.

The $GdFe_3(BO_3)_4$ dielectric has in the ground state the localized *d* electrons of Fe^{3+} in FeO_6 octahedra and the localized *f* electrons of Gd^{3+} in GdO_6 prisms. Inside the BO_3 group, a strong *sp* hybridization of boron and oxygen orbitals takes place. At the same time, the hybridization of the *d* electrons in Fe with the *sp* electrons in BO_3 is extremely weak (as follows from the calculations of the band structure of $FeBO_3$ [15, 16]).

In the one-electron approach based on *ab initio* calculations, the partially filled d^5 terms of Fe^{3+} and f^7 terms of Gd^{3+} would lead to partially filled bands and, hence, to the metallic state. However, due to strong electron correlations, both the *d* and *f* electrons are in the regime of the Mott-Hubbard dielectric. Therefore, the many-electron approach taking strong electron correlations into account is required to describe adequately the electronic structure and optical properties of $GdFe_3(BO_3)_4$.

A strong boron-oxygen hybridization in the BO_3 triangle determines the splitting of bonding and antibonding molecular orbitals that form the top E_v of the filled valence band and the bottom E_c of the empty conduction band. The energy gap between them for $GdFe_3(BO_3)_4$ $E_{go} = E_c - E_v = 3.1$ eV is somewhat greater than that in the $FeBO_3$ crystal (2.9 eV) because the smaller B–O distance in the first crystal leads to a stronger hybridization (see table).

The one-electron scheme of the valence band and the conduction band is overlapped by the single-particle *d* and *f* electron resonances with energies

$$\Omega_d = E(d^{n+1}) - E(d^n), \quad \Omega_f = E(f^{n+1}) - E(f^n),$$

where $E(d^n)$ and $E(f^n)$ are the energies of many-electron terms of iron and gadolinium. These energies are calculated taking into account the effects of strong electron correlations [13]. Because the hybridization for Fe–O and Gd–O is weak, the levels Ω virtually do not interact with the *sp* bands of the BO_3 group.

Because the Gd^{3+} ion does not absorb at energies $h\omega$ below 4 eV, the filled level $\Omega_{fv} = E(f^7) - E(f^6)$ lies below this energy, while the empty level $\Omega_{fc} = E(f^8) - E(f^7)$ lies above this energy. Therefore, only the *d* states of iron are located within the forbidden gap E_g, and in this sense the electronic structures of $FeBO_3$ and $GdFe_3(BO_3)_4$ are similar in this energy range. Moreover, because the Fe–O bond lengths in the FeO_6 octahedra in $FeBO_3$ and $GdFe_3(BO_3)_4$ crystals are close (see table), one can expect a similarity of the Racah parameters *A*, *B*, *C* and the cubic component of the crystal field $\Delta = \varepsilon_d(e_g) - \varepsilon_d(t_{2g})$ for the iron ion. The ground-level energies of the d^n configurations, taking strong electronic configurations into account, are expressed in terms of these parameters as [11, 17]

$$\begin{aligned} E(^5E_1, d^4) &= 4\varepsilon_d + 6A - 21B - 0.6\Delta, \\ E(^6A_1, d^5) &= 5\varepsilon_d + 10A - 35B, \\ E(^5T_2, d^6) &= 6\varepsilon_d + 15A - 21B - 0.4\Delta. \end{aligned} \qquad (4)$$

Here, ε_d is the one-electron energy of the *d* electron in an atom. For the t_{2g} and e_g orbitals in a cubic crystal field, this level splits into $\varepsilon_d(t_{2g}) = \varepsilon_d - 0.4\Delta$ and $\varepsilon_d(e_g) = \varepsilon_d + 0.6\Delta$. The Racah parameters in a crystal field depend on the number of the *d* electrons in the d^n configuration. However, this dependence is rather weak

and therefore can be neglected for simplicity. As in $FeBO_3$, the absorption spectrum of the $GdFe_3(BO_3)_4$ crystal at $\hbar\omega < E_g$ is determined by the *d–d* transitions in the Fe^{3+} ion (excitons) with the energies

$$\begin{aligned}\varepsilon_A &= E(^4T_1) - E(^6A_1),\\ \varepsilon_B &= E(^4T_2) - E(^6A_1),\\ \varepsilon_C &= E(^4E_1) - E(^6A_1) \text{ or } {}^4A_1.\end{aligned} \tag{5}$$

A comparison of the absorption spectra of $FeBO_3$ and $GdFe_3(BO_3)_4$ at normal pressure shows (Fig. 4) that the energies of these excitons coincide, which confirms that the Racah parameters and crystal-field parameters are coincident for these two crystals. These parameters are [11, 18]: $A = 3.42$ eV, $B = 0.084$ eV, $C = 0.39$ eV, and $\Delta = 1.57$ eV.

The great intensity of the absorption band *C* in the spectrum of $GdFe_3(BO_3)_4$, as in the case of $FeBO_3$, can be explained by the overlap of the charge-transfer absorption due to the $p^6d^5 \longrightarrow p^5d^6$ process. The creation of an additional electron in the $Fe^{3+} \longrightarrow Fe^{2+}$ transition requires the energy

$$\Omega_c = E(^5T_2, d^6) - E(^6A_1, d^5), \tag{6}$$

while the annihilation of an electron (creation of a hole) in the $Fe^{3+} \longrightarrow Fe^{4+}$ transition requires the energy

$$\Omega_v = E(^6A_1, d^5) - E(^5E_1, d^4). \tag{7}$$

The Ω_c and Ω_v levels have the meaning of the upper and lower Hubbard subbands and can be expressed in terms of the Racah parameters in the form

$$\begin{aligned}\Omega_c &= \varepsilon_d + 5A + 14B - 0.4\Delta,\\ \Omega_v &= \varepsilon_d + 4A - 14B + 0.6\Delta.\end{aligned} \tag{8}$$

The difference between them (or splitting) is determined by the effective Hubbard parameter,

$$\begin{aligned}U_{\text{eff}} &= \Omega_c - \Omega_n = E_0(d^4) + E_0(d^6)\\ &- 2E_0(d^5) = A + 28B - \Delta = 4.2 \text{ eV}.\end{aligned} \tag{9}$$

The analysis of behavior of the optical spectra of the $FeBO_3$ crystal at high pressures showed [13] that the crystal field increases with pressure, whereas the Hubbard subbands broaden only slightly. As the crystal field increases, the energy of high-spin terms of iron ions almost does not change, while the energy of low-spin states decreases. For $P = 47$ GPa, this leads to the crossover of the terms, which is accompanied by the magnetic collapse and a jumpwise change in electronic and transport properties [13].

The similarity of the electronic structures of the $GdFe_3(BO_3)_4$ and $FeBO_3$ crystals suggests that the electronic transition that we found in the $GdFe_3(BO_3)_4$ crystal at $P_{c2} = 43$ GPa is also related to the spin crossover and the values of critical pressures for both crystals are close (Fig. 6).

However, these crystals also reveal some differences at high pressures. First, we found the structural and optical transitions in $GdFe_3(BO_3)_4$ at 26 GPa, which were not observed in $FeBO_3$. Because the crystal structure of $GdFe_3(BO_3)_4$ is more complicated, the presence of the additional transitions in this crystal is not surprising. The theory [11, 13, 14] considered the pressure-induced variation in the electronic properties only for a specific crystal lattice, and it cannot explain the transition at 26 GPa. To do this, the total energy of the crystal should be calculated, as was done for $FeBO_3$ [19].

The second difference is related to magnetic properties. It is also caused by the more complicated crystal structure of $GdFe_3(BO_3)_4$, where the chains of oxygen-octahedral-containing iron are weakly coupled, and the exchange interaction between neighboring iron atoms involves a long chain of intermediate atoms, being therefore much weaker than in $FeBO_3$. Indeed, the Néel temperature in $GdFe_3(BO_3)_4$ $T_N = 38$ K is an order of magnitude lower than that in $FeBO_3$ ($T_N = 350$ K). The Mössbauer spectra in the $FeBO_3$ crystal at room temperature reveal a magnetically ordered state at the low-pressure phase [20], and the magnetic collapse at the transition point P_c is manifested as the disappearance of the magnetic order parameter owing to a drastic decrease of T_N at the high-pressure phase during the spin crossover. Unlike $FeBO_3$, the spin crossover in the $GdFe_3(BO_3)_4$ crystal, which is observed from optical spectra at room temperature, occurs against the background of the paramagnetic state and is not a real (magnetic) phase transition. At the crossover point, the effective magnetic moment of the Fe^{3+} ion changes, which can be observed by the jumpwise change in the slope of the temperature dependence of the inverse magnetic susceptibility and by Mössbauer spectra. We plan to perform such studies in the near future.

This work was supported by the Russian Foundation for Basic Research (project nos. 02-02-17364a, 03-02-16286a, 04-02-26679, and 04-02-16945a) and the Program of the Department of Physical Sciences, RAS, "Strongly Correlated Electrons." A.M.P. thanks the Foundation for Support of Russian Science for support.

REFERENCES

1. J. A. Campá, C. Cascales, E. Gutierrez-Puebla, *et al.*, Chem. Mater. **9**, 237 (1997).
2. N. I. Leonyuk and L. I. Leonyuk, Prog. Cryst. Growth Charact. Mater. **31**, 179 (1995).
3. N. I. Leonyuk, Prog. Cryst. Growth Charact. Mater. **31**, 279 (1995).
4. D. Jaque, J. Alloys Compd. **323–324**, 204 (2001).
5. M. Huang, Y. Chen, X. Chen, *et al.*, Opt. Commun. **208**, 163 (2002).

6. X. Chen, Z. Luo, D. Jaque, *et al.*, J. Phys.: Condens. Matter **13**, 1171 (2001).
7. A. D. Balaev, L. N. Bezmaternykh, I. A. Gudim, *et al.*, J. Magn. Magn. Mater. **258–259**, 532 (2003).
8. A. D. Balaev, L. N. Bezmaternykh, A. D. Vasil'ev, *et al.*, J. Magn. Magn. Mater. **272–276** (Suppl. 1), E359 (2004).
9. R. Z. Levitin, E. A. Popova, R. M. Chtsherbov, *et al.*, Pis'ma Zh. Éksp. Teor. Fiz. **79**, 531 (2004) [JETP Lett. **79**, 423 (2004)].
10. L. N. Bezmaternykh, S. A. Kharlamova, and V. L. Temerov, Crystallogr. Rep. **49**, 855 (2004).
11. S. G. Ovchinnikov and V. N. Zabluda, Zh. Éksp. Teor. Fiz. **125**, 150 (2004) [JETP **98**, 135 (2004)].
12. E. P. Chukalina, D. Yu. Kuritsin, M. N. Popova, *et al.*, Phys. Lett. A **322**, 239 (2004).
13. A. G. Gavrilyuk, I. A. Troyan, S. G. Ovchinnikov, *et al.*, Zh. Éksp. Teor. Fiz. **126** (3), 650 (2004) [JETP **99**, 566 (2004)].
14. S. G. Ovchinnikov, Pis'ma Zh. Éksp. Teor. Fiz. **77**, 808 (2003) [JETP Lett. **77**, 676 (2003)].
15. A. V. Postnikov, S. T. Bartkowski, M. Neumann, *et al.*, Phys. Rev. B **50**, 14 849 (1994).
16. N. B. Ivanova, V. V. Rudenko, A. D. Balaev, *et al.*, Zh. Éksp. Teor. Fiz. **121**, 354 (2002) [JETP **94**, 299 (2002)].
17. D. T. Sviridov, R. K. Sviridova, and Yu. F. Smirnov, *Optical Spectra of Transition-Metal Ions in Crystals* (Nauka, Moscow, 1976), p. 356 [in Russian].
18. I. S. Édel'man and A. V. Malakhovskiĭ, Opt. Spektrosk. **35**, 959 (1973).
19. K. Parlinski, Eur. Phys. J. B **27**, 283 (2002).
20. V. A. Sarkisyan, I. A. Troyan, I. S. Lyubutin, *et al.*, Pis'ma Zh. Éksp. Teor. Fiz. **76**, 788 (2002) [JETP Lett. **76**, 664 (2002)].

Translated by M. Sapozhnikov